

Examining the implications of photochemical indicators on the O₃-NO_x-VOC sensitivity and control strategies: A case study in the Yangtze River Delta (YRD), China

Xun Li¹, Momei Qin¹, Lin Li¹, Kangjia Gong¹, Huizhong Shen², Jingyi Li¹, Jianlin Hu¹

¹Jiangsu Key Laboratory of Atmospheric Environment Monitoring and Pollution Control, Collaborative Innovation Center of Atmospheric Environment and Equipment Technology, Nanjing University of Information Science and Technology, Nanjing 210044, China

²School of Environmental Sciences and Engineering, Southern University of Science and Technology, Shenzhen, 518055, China

Correspondence to: Momei Qin (momei.qin@nuist.edu.cn); Jianlin Hu (jianlinhu@nuist.edu.cn)

Abstract. Ozone (O₃) has become a significant air pollutant in China in recent years. O₃ abatement is challenging due to the nonlinear response of O₃ to precursors nitrogen oxides (NO_x) and volatile organic compounds (VOCs). Photochemical indicators are widely used to estimate the O₃-NO_x-VOC sensitivity, and this has important policy implications. However, the effectiveness of the indicators has seldom been evaluated. This study examined the applications of four indicators that include the ratio of the production rates of H₂O₂ and HNO₃ (P_{H₂O₂}/P_{HNO₃}), HCHO/NO₂, HCHO/NO_y, and reactive nitrogen (NO_y) in the Yangtze River Delta (YRD) with localized thresholds. The overall accuracy was high (> 92%) for all indicators and not significantly reduced with different simulation periods or in different locations of the region. By comparing with the O₃ isopleths, it was found that HCHO/NO₂ and HCHO/NO_y showed the most consistency, whereas P_{H₂O₂}/P_{HNO₃} (NO_y) tended to underestimate (overestimate) the positive response of O₃ to NO_x. Additionally, P_{H₂O₂}/P_{HNO₃} was less likely to attribute the O₃ formation to mixed sensitivity than the other indicators, and this demonstrated a preference for a single-pollutant control strategy. This study also revealed that the details in the methodology used to derive the threshold values impacted the results, and this may produce uncertainties in the application of photochemical indicators.

1 Introduction

Ozone (O₃) is one of the most important pollutants in the atmosphere, high concentrations of which pose a serious threat to human health, ecosystems, and global climate change (Wang et al., 2020b; Liang et al., 2019; De Marco et al., 2022; Feng et al., 2022; Skeie et al., 2020). Many metropolitan areas in China, such as Beijing-Tianjin-Hebei (BTH), the Yangtze River Delta (YRD), and Pearl River Delta (PRD), have been experiencing severe O₃ pollution in recent years (Gao et al., 2017; Lu et al., 2018). Moreover, unlike the decline in fine particulate matter (PM_{2.5}), the O₃ concentrations in urban areas have increased

(Wang et al., 2019; Lu et al., 2020; Li et al., 2020).

30

O₃ is produced by photochemical reactions involving nitrogen oxides (NO_x) and volatile organic compounds (VOCs). However, the response of O₃ to either precursor is nonlinear due to the changing roles of NO_x and VOCs with different VOC/NO_x ratios in O₃ chemistry, making O₃ pollution abatement more challenging (Wang et al., 2011; Liu et al., 2013). Briefly, when O₃ increases with a reduction (increase) in NO_x (VOCs), O₃ formation is in a NO_x-saturated or VOC-limited regime that tends to occur in urban areas or cold seasons with relatively lower VOC/NO_x ratios (Tan et al., 2018; Sillman, 1995). Conversely, O₃ decreases with reduced NO_x and is typically insensitive to VOC levels in a NO_x-limited regime. This is often the case in rural and remote regions with lower NO_x emissions (Murphy et al., 2007; Sillman, 1999). Importantly, a reduction in either NO_x or VOCs can lead to less O₃ production when the O₃ formation regime is shifted from one to the other, and this is referred to as the transitional regime (Chen et al., 2021; Jin and Holloway, 2015).

40

Many approaches, including photochemical indicators, the observation-based modeling method (OBM), and the emission-based method (EBM) have been developed to predict the O₃-NO_x-VOC sensitivity (Sillman, 2002; Wang et al., 2020a; Shen et al., 2021). Among these approaches, the values of the photochemical indicators (such as VOC/NO_x, the ratios of hydrogen peroxide to nitric acid (H₂O₂/HNO₃) or production rates of H₂O₂ and HNO₃ (P_{H₂O₂}/P_{HNO₃}), the ratios of formaldehyde to nitrogen dioxide or reactive nitrogen (HCHO/NO₂ or HCHO/NO_y), the O₃ to nitric acid ratios (O₃/HNO₃), and NO_y) can be derived directly from ground-based measurements, chemical transport models, or even satellite measurements if available, and thus have been widely used in previous studies (Martin et al., 2004; Jin and Holloway, 2015; Jiménez and Baldasano, 2004; Sillman, 2002; Liu et al., 2010b). For instance, Ye et al. (2021) presented hourly H₂O₂/NO_z (NO_z = NO_y – NO_x) ratios based on the measurements at Mount Tai and found that O₃ formation was VOC-limited in the morning (H₂O₂/NO_z<0.15) and switched to NO_x-limited (H₂O₂/NO_z>0.2) in the afternoon. The ratio H₂O₂/HNO₃ is considered one of the most robust indicators to determine O₃ sensitivity, while the thresholds are highly variable for different regions (Peng et al., 2011; Xie et al., 2014; Ye et al., 2016). P_{H₂O₂}/P_{HNO₃} is primarily used in modeling work, such as the spatial distribution of O₃ formation regimes over the modeling domain that was exhibited with the indicator (Liu et al., 2010a; Du et al., 2022; Zhang et al., 2020). Based on long-term measurements of HCHO and NO₂ columns from satellites, Jin and Holloway (2015) found that near-surface O₃ formation in several megacities in China had changed from VOC-limited in 2005 to transitional in 2013 with reduced NO₂.

50

55

60

The thresholds of photochemical indicators that split VOC-limited, transitional, and NO_x-limited regimes vary from region to region, largely depending on local emissions and possibly related to meteorological conditions as well. It was found that the primary emissions of HCHO increased the value of HCHO/NO₂, and therefore, the O₃ sensitivity determined by the ratio could

65 have been biased with given thresholds. For example, some VOC-limited regimes are misclassified as transitional (Liu et al., 2021). Du et al. (2022) compared the spatial distribution of O₃ sensitivity regimes diagnosed using different indicators and pointed out that P_{H₂O₂}/P_{HNO₃} could be more affected by local emissions than HCHO/NO₂. As H₂O₂ and HNO₃ are very soluble and susceptible to deposition and aerosol formation, the indicator values that involve the two species may change with the meteorological conditions (Castell et al., 2009). However, certain thresholds were often used without considering the variability, such as the range of one to two for HCHO/NO₂ (Jin and Holloway, 2015; Tang et al., 2012; Ma et al., 2021). In particular, the integrated source apportionment method (ISAM) implemented in the community multiscale air quality model (CMAQ) attributes O₃ production to either VOC or NO_x tracers based on a comparison of the instantaneous P_{H₂O₂}/P_{HNO₃} with 0.35, and this ultimately affects the source apportionment of O₃ using ISAM (Kwok et al., 2015). Whether photochemical indicators can accurately predict O₃ sensitivity to precursors with given threshold values has seldom been examined.

75 In light of the above, this work aimed to revisit the effectiveness of photochemical indicators in the prediction of the O₃-precursor response based on a case study in the YRD region in Eastern China. Specifically, the work deployed the mostly-used method to derive localized thresholds of the four photochemical indicators (i.e., P_{H₂O₂}/P_{HNO₃}, HCHO/NO₂, HCHO/NO_y, and NO_y) for Jiangsu Province in the YRD that has been experiencing severe photochemical pollution (Qin et al., 2021; Xu et al., 2021; Lu et al., 2018). The assessment was conducted to examine three aspects: (1) whether the localized threshold values are appropriate for a different location or a different year; (2) the consistency of the photochemical indicator approach with O₃ isopleths plots for predicting the O₃-NO_x-VOC response; and (3) possible uncertainties induced by the methodology with which the threshold values are determined. This work can provide insight into the use of photochemical indicators in understanding O₃ formation and making effective strategies for emission control.

2 Methods

2.1 Model configurations

85 The CMAQ model version 5.2 was applied to simulate the photochemical pollution over the YRD and its surrounding areas (Fig. 1) in July 2017. The simulation was performed at a 4-km resolution, using the chemical mechanism of saprc07tic. A regional O₃ pollution event that occurred from July 22 to 31 with the mean level of the observed daily maximum 8-hr average (MDA8) O₃ exceeding 85 ppb over the YRD was selected to study the relationship between the O₃-NO_x-VOC sensitivity and the values of the photochemical indicators. The CMAQ model was driven by a mesoscale meteorological model, the Weather Research and Forecasting (WRF) version 4.2.2. The 2017 emission inventory of anthropogenic air pollutants in the YRD compiled by the Shanghai Academy of Environmental Sciences (An et al., 2021) was adopted, with the details of the other emissions (i.e., biogenic emissions and open burning) found in Hu et al. (2016).



Figure 1: The simulation domain. The blue area indicates the YRD including Jiangsu, Anhui, Shanghai, and Zhejiang. Three representative sites of Caochangmen (CCM), Zhonghuamen (ZHM), and Laoshan (LS) are marked.

95 2.2 Model performance evaluation

The model performance on O_3 was examined by comparing the simulation with observational data at the monitoring sites supervised by the China National Environmental Monitoring Center (CNEMC) in 13 cities in Jiangsu Province. Three metrics (the normalized mean bias (NMB), the normalized mean error (NME), and the correlation coefficient (r)) as in Sheng et al. (2022) were calculated to evaluate the agreement between the simulation and observations. The criteria of the model performance were recommended by Emery et al. (2017). Table S1 shows that the NMB (NME) values in 12 (10) out of 13 cities met the criteria, indicating that the overall performance was good. In general, the model overestimated O_3 , with the NMB in the range of -2%–17%. The correlations of the simulation with the observations (all r values above 0.5) indicated that hourly variations in the simulation agree well with the observations. Additionally, three sites in Nanjing (a megacity in Jiangsu), including Caochangmen (CCM), Zhonghuamen (ZHM), and Laoshan (LS), representing downtown, upwind, and downwind areas of the city (see Fig. 1), respectively, were selected to examine the consistency between the photochemical indicators and the O_3 isopleths in the implication of O_3 -precursor sensitivities. Figure S1 shows that the model well reproduced the O_3 pollution events at the three sites during the simulation period.

Other species involved in the photochemical indicators, such as HCHO, HNO_3 , NO_2 , and NO_y (NO_y

110 (g)=NO+NO₂+NO₃+2×N₂O₅+HONO+HNO₃+HNO₄+peroxyacetyl nitrate and its homologs (PANs)+alkyl nitrates (ANs) and
nitrogen oxychlorides (ClNO_x) in the model), were examined and compared with observations during the EXPLORE-YRD
campaign (Li et al., 2021; Sun et al., 2022). Figure S2 shows that HCHO was underestimated by 51%, while NO₂ and NO_y
were slightly overestimated, with NMBs of 16% and 7%, respectively. The anthropogenic emission inventory and model were
set up as in the simulation for the EXPLORE-YRD campaign, and the simulated ratios of HCHO/NO₂ and HCHO/NO_y in this
115 study could have been underestimated. In addition, the simulation could represent an environment with less abundant VOCs
than in the real atmosphere over the YRD.

2.3 Determination of the indicator thresholds

The use of photochemical indicators requires threshold values that differentiate O₃ formation regimes. In this study, the
thresholds of the indicators were derived based on the association of the O₃ reduction relative to the baseline emission scenario
resulting from NO_x or VOC emission reductions (i.e., ΔO_{3 NOx} or ΔO_{3 VOC}), with concurrent indicator values at all grid cells in
120 Jiangsu Province. Therefore, two additional runs with either a 35% decrease in NO_x or a 35% decrease in VOC emissions were
performed following Sillman et al. (1998) and other studies (Xie et al., 2014; Peng et al., 2011). The resulting O₃ changes (ΔO<sub>3
NOx</sub> and ΔO_{3 VOC}) were obtained to identify the O₃ formation regimes at each grid cell, with the criteria given in Table 1. It
should be noted that the average changes in O₃ during 1–4 p.m. during the simulation period were used when O₃ peaked and
125 was of most concern.

**Table 1: Identification of the O₃ formation regimes at each grid cell based on the O₃ changes resulting from perturbed emissions as
in Sillman et al. (1998) or the sensitivity coefficients using the high-order decoupled direct method (HDDM) as in Wang et al. (2011).**

Method	O ₃ formation regime	Definition
Perturbed simulations	VOC-limited	ΔO _{3 VOC} ≥ 5 ppb and (ΔO _{3 VOC} - ΔO _{3 NOx}) ≥ 5 ppb
	NO _x -limited	ΔO _{3 NOx} ≥ 5 ppb and (ΔO _{3 NOx} - ΔO _{3 VOC}) ≥ 5 ppb
High-order decoupled direct method (HDDM)	VOC-limited	S ¹ _{VOCs} ≥ 5 ppb and (S ¹ _{VOCs} - S ¹ _{NOx}) ≥ 5 ppb
	NO _x -limited	S ¹ _{NOx} ≥ 5ppb and (S ¹ _{NOx} - S ¹ _{VOCs}) ≥ 5 ppb

130 This study focused on four photochemical indicators that are frequently used, including P_{H2O2}/P_{HNO3}, HCHO/NO₂, HCHO/NO_y,
and NO_y, with the underlying mechanisms extensively described in the literature (Xie et al., 2014; Kwok et al., 2015; Sillman,
1995; Duncan et al., 2010). The indicator values for each grid cell were calculated based on the simulated concentrations of
related species, except for P_{H2O2}/P_{HNO3}, which were obtained using the integrated reaction rate (IRR) of the CMAQ process
analysis tool (Gipson and Young, 1999). The percentile distribution of the indicator values for the VOC-limited grid cells and
135 the NO_x-limited grid cells were examined individually. The photochemical indicators typically showed higher values at NO_x-
limited grid cells than in VOC-limited locations. Finally, the thresholds of a certain indicator were determined using the 95th

percentile value of the indicator for the VOC-limited grid cells and the 5th percentile value for the NO_x-limited grid cells as the lower and upper limits of the transition intervals, respectively. Indicator values lower than the transition intervals suggested O₃ formation was VOC-limited, while higher values than the transition intervals were associated with NO_x-limited regimes. In some cases, the 95th percentile VOC-limited value was higher than the 5th percentile NO_x-limited value, indicating the indicator was invalid and could not be used to determine the O₃ sensitivity properly.

2.4 Evaluation of the indicators

2.4.1 Evaluation metrics

The feasibility of a given threshold for an indicator applied throughout a region, or over a short-term period (the order of 1–2 years) was evaluated in this study. Some metrics have been developed to estimate the uncertainties in the determination of O₃ regimes using photochemical indicators (Wang et al., 2011; Ye et al., 2016). This work applied Error A, Error B, and the overall accuracy (OA) in Ye et al. (2016) for the evaluation, with the equations given in Table 2. For example, the ErrA_NO_x describes the situation where among all grid cells (colored areas in Fig. 2d) with indicator values higher than the upper limit of the transition interval (i.e., assigned to NO_x-limited regimes with the indicator), there existed VOC-limited grid cells that were incorrectly assigned to the NO_x-limited regime. ErrB_NO_x estimates the fraction of the NO_x-limited grid cells (blue areas in Fig. 2d) that were not classified as a NO_x-limited regime since the corresponding indicator values were lower than the upper threshold. ErrA_VOC and ErrB_VOC were defined analogously. OA describes the fraction of all correctly classified grid cells using the indicator at all VOC- or NO_x-limited grid cells.

Table 2: Metrics of the indicator performance evaluation provided in Ye et al. (2016).

Metric	Equation
Error A_NO _x	$\frac{\text{Number of VOC-limited grid cells with indicator values above the upper threshold}}{\text{Number of all NO}_x\text{-limited and VOC-limited grid cells with indicator values above the upper threshold}} \times 100\%$
Error B_NO _x	$\frac{\text{Number of NO}_x\text{-limited grid cells with indicator values below the upper threshold}}{\text{Number of all NO}_x\text{-limited grid cells}} \times 100\%$
Error A_VOC	$\frac{\text{Number of NO}_x\text{-limited grid cells with indicator values below the lower threshold}}{\text{Number of all NO}_x\text{-limited and VOC-limited grid cells with indicator values below the lower threshold}} \times 100\%$
Error B_VOC	$\frac{\text{Number of VOC-limited grid cells with indicator values above the lower threshold}}{\text{Number of all VOC-limited grid cells}} \times 100\%$
OA	$OA = \left(\frac{\text{Number of VOC-limited grid cells with indicator values below the lower threshold} + \text{Number of NO}_x\text{-limited grid cells with indicator values above the upper threshold}}{\text{Number of all NO}_x\text{-limited and VOC-limited grid cells}} \right) \times 100\%$

The indicator evaluation was conducted for the simulation in 2017 (see section 2.1). Additionally, a simulation for the same period (over July 22–31) in 2018, which has an identical model configuration and inputs in all aspects except for the

meteorology, was performed for the evaluation as well. Thus, applications of the photochemical indicators with derived thresholds in a different location within the region, in a different year, or with changes in both, can be examined separately. This provided insight into the uncertainties associated with emissions or meteorology.

2.4.2 O₃ isopleths

The O₃-NO_x-VOC sensitivity determined by photochemical indicators was compared with the O₃ isopleths that describe the nonlinear relationship between O₃ and the precursors and inform decision-makers of emission control strategies in a different manner. The response of O₃ to the domain-wide reductions in VOC and NO_x emissions at three representative sites (CCM, ZHM, and LS) during 1–4 p.m. during the simulation period was investigated. Specifically, a total of 36 emission scenarios with anthropogenic VOC and NO_x emissions reduced by 0, 20, 40, 60, 80, and 100%, both singly and in combination were simulated to construct the O₃ isopleth diagram. The O₃ formation regimes based on the thresholds derived in section 2.3 were indicated with color and overlapped with the isopleths.

2.5 Uncertainties in the thresholds

In section 2.3, the O₃ formation regimes were presumably identified according to changes in O₃ with the emission reductions, while the rules could be different in detail. For example, Liang et al. (2006) examined changes in the 8-hr O₃ with a 25% reduction in VOC or NO_x emissions instead of the 1-hr O₃ with 35% reductions, as in Sillman (1995). Accordingly, the criteria changed from 5 ppb to 2.5 ppb. Zhang et al. (2020) explored the correlation of indicator values with the relative O₃ changes resulting from a 50% reduction in the NO_x or VOC emissions. Du et al. (2022) applied the decoupled direct method (DDM) to investigate the sensitivity of O₃ to precursors, instead of perturbing emissions. The impacts on the derived thresholds of the indicators were explored by conducting a few individual tests:

- (1) The criteria for the O₃ reduction (see Table 1) were set at 2 ppb, 3 ppb, and 6 ppb.
- (2) The relative changes in O₃ were examined using the criteria of 2%, 5%, and 8% instead of an absolute change of 5 ppb.
- (3) The 35% emission reduction scenarios were replaced with a 20% and a 40% reduction in the VOC or NO_x emissions.
- (4) The high-order decoupled direct method (HDDM) was adopted to split the O₃ formation regimes in two manners referred to as “DDM1” and “DDM2”. The HDDM can quantify the responsiveness of air pollutants to infinitesimal perturbations of a model parameter or input (e.g., an emission rate of a precursor) with sensitivity coefficients (Cohan et al., 2005). In this study, the HDDM estimated the first- and second-order sensitivity coefficients of O₃ to NO_x and VOCs (i.e., $S_{\text{NO}_x}^1$, S_{VOCs}^1 , $S_{\text{NO}_x}^2$, S_{VOCs}^2). With the DDM1 approach, the NO_x-limited locations were defined as those grid cells where $S_{\text{NO}_x}^1$ was higher than 5 ppb and at least 5 ppb higher than S_{VOCs}^1 (Table 1), following Wang et al. (2011). The VOC-limited grid cells were defined similarly. The DDM2 approach estimated O₃ changes with 35% reductions in emissions via the Taylor series expansions (Cohan et al., 2005) instead of the perturbed simulations.

3 Results and discussion

3.1 Threshold values of the photochemical indicators

The changes in the O_3 concentrations when reducing VOC or NO_x emissions were used to determine the O_3 formation regimes. Figure 2a shows that high O_3 concentrations (averaged from 1 to 4 p.m. during July 22–31) primarily occurred along the Yangtze River and southern Jiangsu, and O_3 in northern Jiangsu was relatively low. The NO_x emission reduction predominantly led to O_3 decreases in Jiangsu, while only a few locations, such as near the estuary of the Yangtze River, showed an increased O_3 relative to the base case (Fig. 2b). The VOCs emission reductions resulted in less significant O_3 decreases compared to the NO_x reduction scenario (Fig. 2c). The O_3 sensitivity regime for each grid cell in Jiangsu was identified with the method depicted in section 2.3 (Fig. 2d). The O_3 formation in central and southern Jiangsu, where O_3 is abundant, is typically NO_x -limited as a result of a relatively low NO_x concentration in the afternoon (Duncan et al., 2010; Jin et al., 2017; Jin and Holloway, 2015). Some areas along (and on) the Yangtze River were characterized to be VOC-limited regimes, with substantial emissions of NO_x from ship emissions and industry (Sheng et al., 2022). However, not all grid cells in Jiangsu were assigned to the VOC- or NO_x -limited regimes. The white areas in Jiangsu in Fig. 2d indicate that O_3 was insensitive to both NO_x and VOCs (i.e., $\Delta O_{3\text{VOC}} < 5$ ppb and $\Delta O_{3\text{NO}_x} < 5$ ppb); alternatively, O_3 was sensitive to NO_x (VOC) emissions but showed small changes in O_3 with the perturbation of NO_x (VOC) relative to the VOC (NO_x) reduction scenario (i.e., $|\Delta O_{3\text{VOC}} - \Delta O_{3\text{NO}_x}| < 5$ ppb).

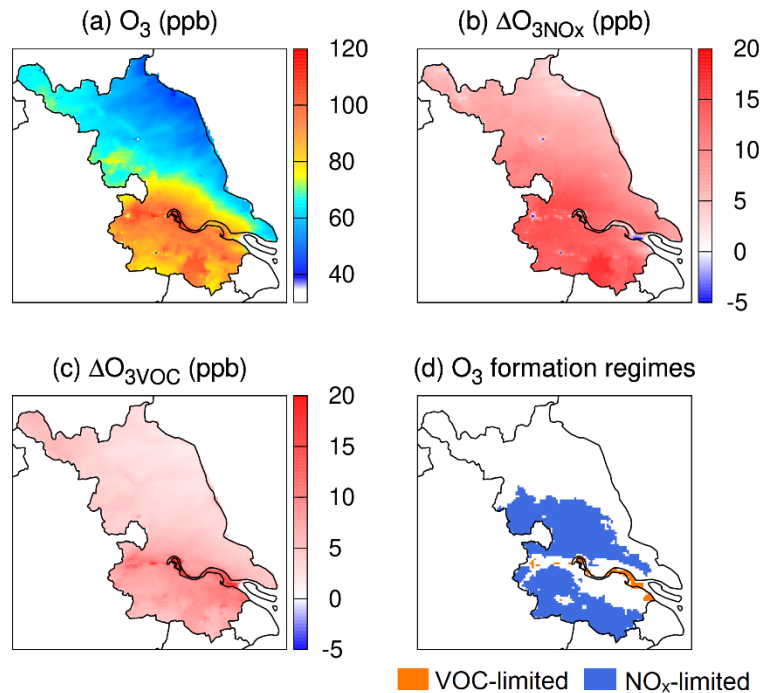


Figure 2: (a) Simulated spatial distribution of O₃ averaged from 1 to 4 p.m. during July 22-31 in Jiangsu Province, (b-c) O₃ reduction due to a 35% reduction in domain-wide NO_x and VOC emissions, respectively, (d) O₃ formation regimes determined with perturbed simulations.

210 The O₃ reductions ($\Delta O_{3\text{NO}_x}$ or $\Delta O_{3\text{VOC}}$) against photochemical indicator values at all grid cells over the domain were examined (Fig. 3). The mean values of the $\Delta O_{3\text{NO}_x}$ slightly increased with higher $P_{\text{H}_2\text{O}_2}/P_{\text{HNO}_3}$, while the $\Delta O_{3\text{VOC}}$ values showed a decreasing trend, indicating that a reduction in NO_x (VOC) emissions became more (less) effective for O₃ abatement in the locations with higher indicator values. Other indicators displayed a similar pattern except for NO_y, which displayed an opposite result. Due to the contrasting dependence of the $\Delta O_{3\text{NO}_x}$ and the $\Delta O_{3\text{VOC}}$ on the indicator values, the thresholds of the

215 the photochemical indicators that separate the O₃ formation regimes were determined (Table 3 and vertical lines in Fig. 3). The localized thresholds for $P_{\text{H}_2\text{O}_2}/P_{\text{HNO}_3}$ (0.55, 0.75) were remarkably higher than that implemented in the model, i.e., 0.35, which would lead to misattribution of the VOC-limited or the transitional regime to the NO_x-limited regime in some locations if the single value was directly used. The thresholds differed from those proposed by researchers in other countries, and some regions in China had significantly distinct thresholds as well (Du et al., 2022; Zhang et al., 2020; Tonnesen and Dennis, 2000a; Liu et

220 al., 2010a).

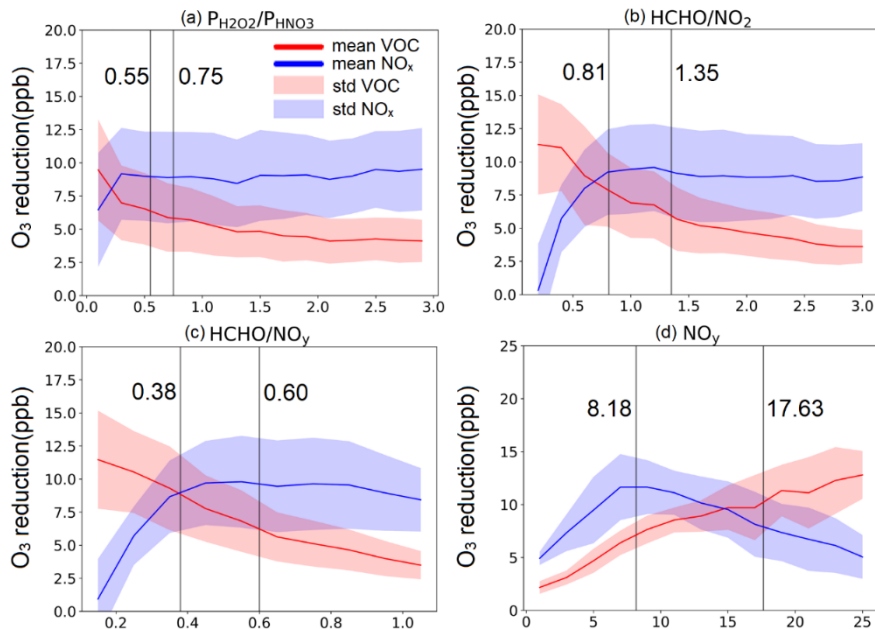


Figure 3: Relationships between the simulated O₃ reductions with the perturbed emissions and concurrent values of $P_{\text{H}_2\text{O}_2}/P_{\text{HNO}_3}$, HCHO/NO_2 , HCHO/NO_y , and NO_y at all the grid cells in the domain. The red (blue) lines represent the average O₃ changes resulting

225 from VOC (NO_x) emission reductions, with the shaded areas for the standard deviations. The thresholds derived in this study (see Table 3, with the method detailed in Section 2.3) are indicated as the grey vertical lines.

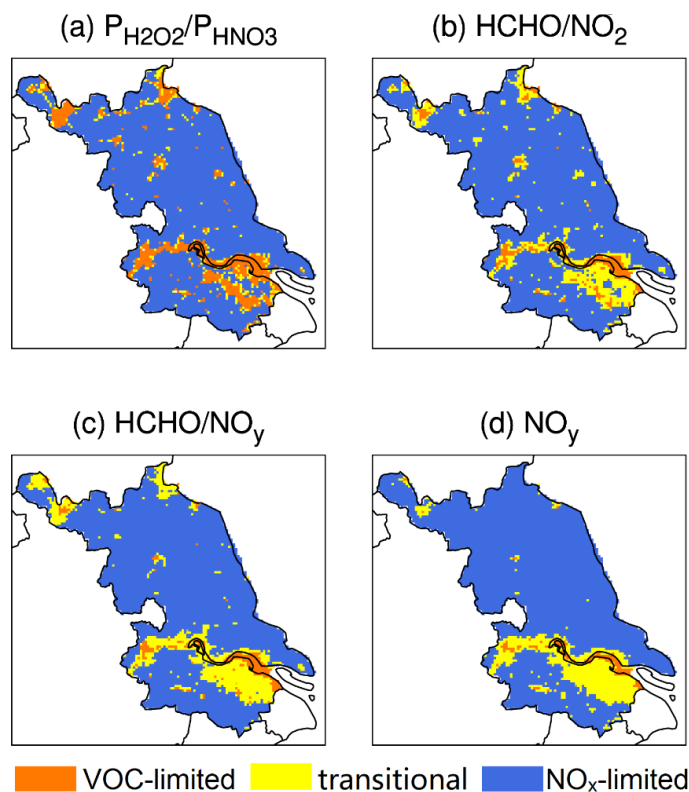
Table 3: Thresholds of the indicators derived in this study and reported in previous work.

Indicators	This study	Other studies
P _{H2O2} /P _{HNO3}	(0.55, 0.75)	US: 0.06 (Tonnesen and Dennis, 2000a) China: 0.2 (Liu et al., 2010a) North China Plain: (0.08, 0.2) (Zhang et al., 2020) East China: (0.30, 1.10) (Du et al., 2022)
HCHO/NO ₂ (surface)	(0.81, 1.35)	US: (0.8, 1.8) (Tonnesen and Dennis, 2000b) East Asia: (0.5, 0.8) (Jin et al., 2017) East China: (0.36, 0.45) (Du et al., 2022) Yangtze River Delta: (0.55, 1.0) (Liu et al., 2021)
HCHO/NO _y	(0.38, 0.60)	US: 0.28 (Sillman, 1995) California: (0.5, 0.9) (Lu and Chang, 1998) Pearl River Delta: 0.41 (Ye et al., 2016)
NO _y	(8.18, 17.63)	US: 20 (Sillman, 1995) California: 5 (Lu and Chang, 1998) Germany: 7.78 (Vogel et al., 1999) Mexico City: 8.75 (Torres-Jardon et al., 2009)

230 This work revisited other photochemical indicators including the surface HCHO/NO₂, HCHO/NO_y, and NO_y. The transition interval of HCHO/NO₂ was determined as (0.81, 1.35), showing a higher and wider range than in other work (Jin et al., 2017; Liu et al., 2021; Du et al., 2022), but relatively consistent with Tonnesen and Dennis (2000b). It is worth noting that the values mentioned above are all based on measurements or simulations at the ground level, while column HCHO/NO₂ retrieved from satellite measurements are more widely used, with thresholds of (1, 2) (Jin and Holloway, 2015; Jin et al., 2017; Duncan et al., 2010; Wang et al., 2021). The transition range for the column HCHO/NO₂ is typically broader than that for the surface ratio, e.g., the former of (1.17, 2.42) versus the latter of (0.36, 0.45) in East China (Du et al., 2022). The thresholds of HCHO/NO_y and NO_y in this study were (0.38, 0.60) and (8.18, 17.63), respectively, comparable to the values proposed previously. The comparison shown in Table 3 suggests that the thresholds were mostly location-specific, possibly as they are dependent on atmospheric conditions and emission features. However, the methodology that is used to derive thresholds can also lead to distinct threshold values, and this is discussed in section 3.4.

The spatial distributions of the O₃ formation regimes identified by the photochemical indicators with localized thresholds are

245 exhibited in Fig. 4. Most of the areas in Jiangsu (> 80% of the grid cells covering Jiangsu, Table S2) were attributed to NO_x -limited regimes in terms of the summertime O_3 formation in the afternoon using all indicators. A few urban centers and some locations near the Yangtze River were identified as VOC-limited or transitional regimes where the four indicators largely showed differences. The O_3 formations in these areas were primarily VOC-limited according to $P_{\text{H}_2\text{O}_2}/P_{\text{HNO}_3}$ and showed a transition from VOC-limited to NO_x -limited at the surrounding grid cells. However, other indicators tended to assign the areas along and to the south of the river to transitional regimes. The fraction of the VOC-limited regimes in the area in Jiangsu with $P_{\text{H}_2\text{O}_2}/P_{\text{HNO}_3}$ (~13%) was considerably higher than that using HCHO/NO_2 and HCHO/NO_y (4-5%). NO_y , which is the least impacted by VOC emissions, attributed the least areas to the VOC-limited regimes (~2%) concerning O_3 formation. Accordingly, transitional regimes were the least using $P_{\text{H}_2\text{O}_2}/P_{\text{HNO}_3}$, ~5% compared to 13–15% using HCHO/NO_2 , HCHO/NO_y , and NO_y .



255 **Figure 4: O_3 formation regimes based on the indicator values and thresholds in Table 3. The orange indicates a VOC-limited regime. The blue indicates a NO_x -limited regime. The yellow is associated with a transitional regime.**

3.2 Evaluation of the photochemical indicators

260 Table 4 shows the accuracy of the photochemical indicators in splitting the O₃ formation regimes with thresholds derived in this study. As expected, the ErrB and OA for the application in Jiangsu in 2017 (see the case “Sim_2017+Jiangsu” in Table 4) were approximately 5% and 95%, respectively, as a result of the nature of the method (see section 2.3). The values of ErrA were lower than ErrB, suggesting that chemical regimes determined by the indicator values were largely consistent with that based on O₃ changes when perturbing emissions. However, it is more likely that sensitivities indicated by O₃ changes do not necessarily correspond to indicator values in the correct intervals. Additionally, the ErrA_VOC and ErrA_NO_x for P_{H2O2}/P_{HNO3} were higher than that of the other indicators, likely due to less area associated with mixed O₃ sensitivity using P_{H2O2}/P_{HNO3} (see 265 Table S2), which could increase the chance of misclassification.

Table 4: Evaluation of the photochemical indicators in the YRD (unit of %).

Case	Indicator	ErrA_VOCs	ErrB_VOCs	ErrA_NO _x	ErrB_NO _x	OA
Sim_2017+Jiangsu	P _{H2O2} /P _{HNO3}	3.9	6.6	0.1	5.1	94.8
	HCHO/NO ₂	2.9	5.7	0.0	5.1	94.9
	HCHO/NO _y	0.0	6.6	0.0	4.7	95.2
	NO _y	0.0	5.7	0.0	4.9	95.1
Sim_2017+Other	P _{H2O2} /P _{HNO3}	7.4	0.0	0.0	2.0	98.0
	HCHO/NO ₂	2.2	0.0	0.0	1.7	98.3
	HCHO/NO _y	2.1	0.0	0.0	0.7	99.3
	NO _y	0.0	12.8	0.0	1.3	98.6
Sim_2018+Jiangsu	P _{H2O2} /P _{HNO3}	2.4	0.0	0.0	4.3	96.9
	HCHO/NO ₂	0.0	0.8	0.0	7.0	94.8
	HCHO/NO _y	0.0	0.8	0.0	10.1	92.2
	NO _y	0.0	8.3	0.3	0.3	97.4
Sim_2018+Other	P _{H2O2} /P _{HNO3}	2.7	7.0	0.1	1.7	98.2
	HCHO/NO ₂	6.2	14.3	0.1	1.6	98.0
	HCHO/NO _y	0.5	12.2	0.1	1.2	98.5
	NO _y	0.0	51.3	0.1	1.3	97.3

270

The above evaluation also showed that emissions could have a minor effect on the performance of the indicators on a regional scale. The thresholds derived from the simulation in Jiangsu well identified O₃ sensitivities in other regions of the YRD (see the case “Sim_2017+Other”), where emissions were different (e.g., abundant biogenic VOCs in the southern YRD vs.

275 dominance of anthropogenic emissions in Jiangsu) and with OAs greater than 98% for all the indicators. This suggests that it
is plausible to specify regionwide thresholds for photochemical indicators. In addition, the indicators can generally separate
O₃ formation regimes in Jiangsu for the same period in 2018 (see the case “Sim_2018+Jiangsu”) when the meteorology could
differ from that in 2017. However, HCHO/NO_y and HCHO/NO₂ appeared to be more easily affected by meteorology, as
indicated by the ErrB_NO_x that showed that many NO_x-limited grids had indicator values lower than the upper thresholds. The
OAs were relatively high in the case when both the emissions and meteorology changed (see the case “Sim_2018+Other”),
280 although the ErrB_VOC were remarkably higher. This was due to fewer VOC-limited grids in the YRD, half of which had
indicator values within the transition intervals and thus were misclassified as the transitional regime. The evaluation showed
that indicators could perform better in detecting O₃ formation regimes that were predominant. However, the drawback of the
evaluation is that it does not account for grids that are neither VOC-limited nor NO_x-limited in terms of the O₃ formation based
on the $\Delta O_3_{NO_x}$ or the ΔO_3_{VOC} (i.e., the white area in Jiangsu in Fig. 2d), and the uncertainties of the photochemical indicators
285 in these areas are unknown.

3.3 Consistency with the O₃ isopleths

O₃ formation regimes identified by the indicator values with varied combinations of VOC and NO_x emissions were plotted
together with the O₃ isopleths to examine the indicators for implications in effective emission control strategies. Figure 5 and
Figs. S3–S4 show the comparison at the CCM, ZHM, and LS sites, respectively. As no significant variations were found at the
290 three sites, only the plot for CCM is shown in the main text. The P_{H₂O₂}/P_{HNO₃} value with the base emission points to a VOC-
limited regime at the CCM site, whereas the isopleths suggest that a reduction in the NO_x emissions should lead to reduced O₃.
This also happens in some cases with lower VOC and NO_x emissions, indicating that P_{H₂O₂}/P_{HNO₃} is likely to underestimate
the positive sensitivity of O₃ to NO_x. The indicators were assumed to have constant thresholds that do not change with
emissions; this could partially explain the inconsistency of the indicators with the O₃ isopleths. The P_{H₂O₂}/P_{HNO₃} values at the
295 LS and ZHM sites showed similar results, except that the O₃ formation at LS site shifted from VOC-limited to a transitional
regime earlier with decreasing NO_x emissions than at the other two sites as indicated by the ratio.

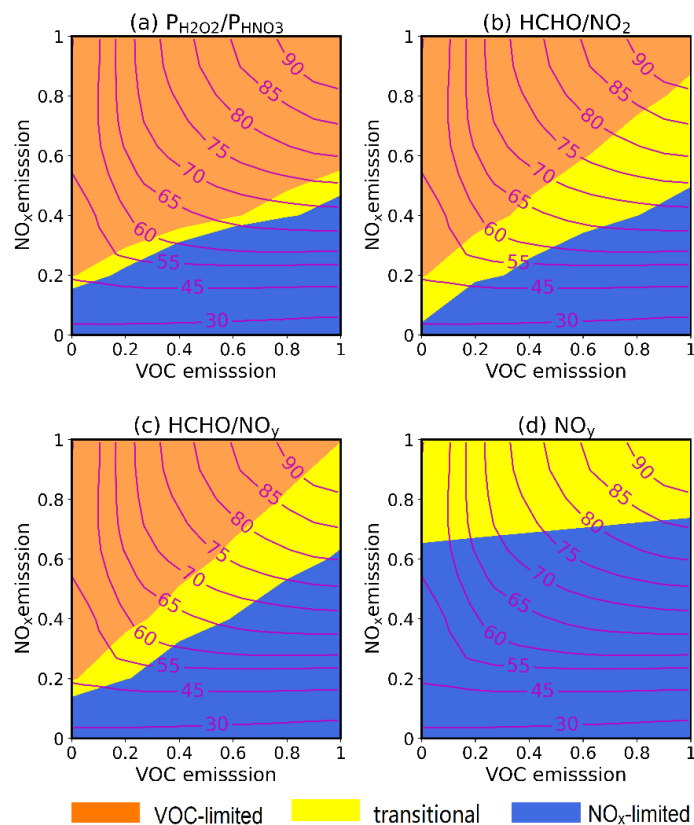


Figure 5: O_3 isopleths (red lines) overlap with the O_3 formation regimes (shading color) identified with $P_{H_2O_2}/P_{HNO_3}$, $HCHO/NO_2$, $HCHO/NO_y$, and NO_y (the thresholds given in Table 3) at the CCM site. The orange indicates a VOC-limited regime. The yellow indicates a transitional regime, and the blue indicates a NO_x -limited regime.

It appears that $HCHO/NO_y$ was the most consistent with the O_3 isopleths among the four indicators, followed by $HCHO/NO_2$. Both $HCHO/NO_y$ and $HCHO/NO_2$ suggest that all three sites resided in transitional regimes under the base emission scenario, except for CCM using $HCHO/NO_2$, which showed that O_3 would respond to NO_x changes negatively. However, $HCHO/NO_y$ and $HCHO/NO_2$ had more emission scenarios assigned to transitional regimes compared with $P_{H_2O_2}/P_{HNO_3}$, which was in agreement with the spatial distributions shown in Fig. 4. This implies that the two indicators emphasize controlling both VOC and NO_x rather than a single pollutant. However, the HCHO levels could be affected by primary emissions (Liu et al., 2021) or highly variable due to the dependence of isoprene on temperature (isoprene dominating HCHO production with intensive biogenic emissions) (Duncan et al., 2010). Therefore, the link between the $HCHO/NO_y$ (or $HCHO/NO_2$) values and the O_3 -VOC- NO_x sensitivity and resulting emission control strategies of anthropogenic precursors (that are controllable) is more uncertain under certain conditions.

315 The O₃ formation at the CCM site was dominated by NO_x-limited regimes based on NO_y, which was predominantly affected by NO_x emissions, and did not show a sole sensitivity to VOCs (Fig. 5d). This was different from other indicators as well as the O₃ isopleths in terms of policy implications. The comparison between the O₃-VOC-NO_x sensitivity revealed by NO_y and the O₃ isopleths showed that the indicator tended to overestimate the response of O₃ to NO_x (i.e., the VOC-limited regimes were misclassified as transitional regimes in the upper left corner of Fig. 5d) or underestimate the O₃-VOC sensitivity (i.e., the transitional regimes were misclassified as NO_x-limited regimes in the middle-left portion of Fig. 5d).

320 **3.4 Uncertainties associated with the methodology**

Apart from local emissions and meteorology that could partially explain the gap between the indicator thresholds proposed earlier and in this work, we found that the methodology to derive the thresholds could be slightly different and the impacts are unknown. Therefore, a series of tests were conducted to examine how those details in the methodology alter the thresholds of P_{H2O2}/P_{HNO3} (Fig. 6) and other indicators (Figures S6-S8).

325

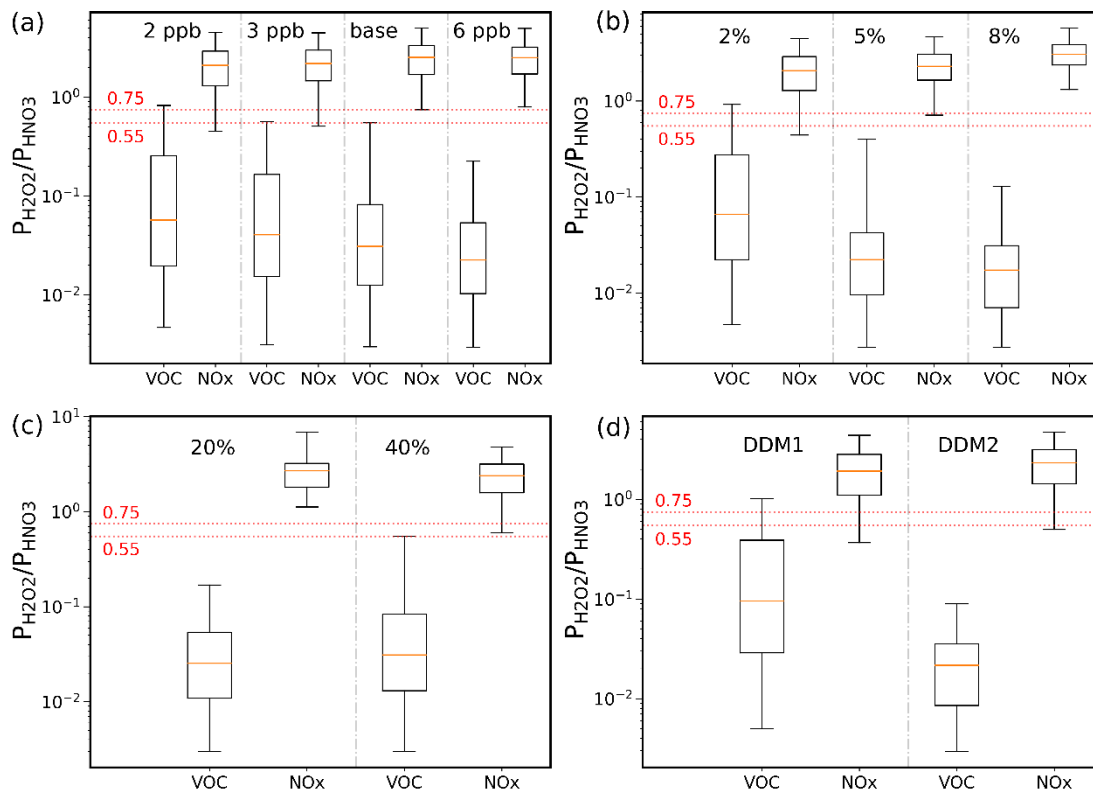


Figure 6: The percentile distributions of the $P_{H_2O_2}/P_{HNO_3}$ values at the VOC- or NO_x-limited grid cells with different setups in

methodology. The boxes indicate the 25th and 75th percentiles of the indicator values with the median values marked with red horizontal lines in the boxes, and the whiskers extend to the 5th and 95th percentiles. In each group, the upper whisker of the box in the VOCs column and the lower whisker of the box in the NO_x column reflect the lower and upper values of the threshold intervals, respectively. The threshold intervals in Table 3 are indicated with red dotted lines.

First, the VOC- (NO_x-) limited grid cells were defined as the locations where the reduction in O₃ as a response to the VOC (NO_x) reduction exceeded the O₃ reduction associated with the reduced NO_x (VOC) by more than 2 ppb, 3 ppb, and 6 ppb instead of the original 5 ppb (see Table 1). The threshold intervals are wider with higher criteria, e.g., the range of (0.3, 0.8) with sensitivity differences of > 6 ppb versus (0.55, 0.75) with > 5 ppb, leading to fewer VOC- or NO_x-limited grid cells based on the indicator and more transitional grid cells with less chance of misclassification (Fig. 6a). However, the sensitivity differences of 2–3 ppb are too small to differentiate sensitivity types of the grid cells using the indicators, as the 95th percentile of the indicator values at the VOC-limited grids is higher than the 5th percentile of the values at the NO_x-limited grids when determining the thresholds (see section 2.3). Hence, the indicators are invalid. Similarly, if the relative changes in O₃ were applied to quantify the O₃-VOC-NO_x sensitivity, such as using the differences of 2%, 5%, or 8% as the criteria, the derived thresholds would be considerably different as well (Fig. 6b). The relative changes make more sense since O₃ changes of ~5 ppb due to a certain amount of VOC or NO_x reduction are less likely to take place in locations with low O₃ than in relatively polluted regions. As a result, the grid cells with low O₃ are seemingly insensitive to precursors and were excluded from the VOC- or NO_x-limited grids that were used to derive the thresholds. This can particularly affect the lower limits of the thresholds with much fewer VOC-limited grids, as in this study, and vice versa.

In Fig. 6c, the VOC and NO_x emissions were individually reduced by 20% or 40% instead of 35%, but with a constant criterion of > 5 ppb for the sensitivity differences. The less reduction in emissions resulted in wider threshold intervals (0.18, 1.12) with a 20% reduction versus (0.55, 0.75) with a 35% reduction, and (0.55, 0.60) with a 40% reduction. This was similar to the case with higher criteria (Fig. 6a). In addition, if the VOC- or NO_x-limited grids were defined based on the S¹_{VOCs} and S¹_{NO_x} in the HDDM (see Table 1 and DDM1 in Fig. 6d), the indicator values for the VOC-limited grids and the NO_x-limited grids would overlap to a large extent, with the 95th percentile of the indicator values at the VOC-limited grids of 1.0, and the 5th percentile of the values at the NO_x-limited grids of 0.37. Therefore, the indicator could not be used. S¹_{VOCs} and S¹_{NO_x} approximate the O₃ changes with a 100% reduction in the VOC and NO_x emissions, respectively, without considering the nonlinearity (i.e., higher-order sensitivities) in O₃ chemistry. This finding is consistent with Fig. 6c which shows a quite narrow range of threshold intervals with more reduction in the precursor emissions. Additionally, the upper and lower thresholds derived with the DDM2 approach were 0.50 and 0.11, lower than 0.75 and 0.55, respectively. This was due to the lower O₃ changes estimated with the second-order Taylor expansions than with the perturbed simulations (Fig. S5), similar to the case with a 20% reduction in the VOC or NO_x emissions, and possibly reflecting the importance of higher-order terms in the HDDM as well. The results of

HCHO/NO₂, HCHO/NO_y, and NO_y (Figures S6-S8) were similar. They all indicated that the thresholds of the photochemical indicators are dependent on the methods or parameters in the methodology. This could be one of the major uncertainties in the application of indicators to determine O₃ chemical regimes.

4 Conclusions

365 This work revisited four photochemical indicators, including P_{H₂O₂}/P_{HNO₃}, HCHO/NO₂, HCHO/NO_y, and NO_y, in implications of the O₃-NO_x-VOC sensitivity and emission control strategies using a case study in the YRD. The threshold intervals for Jiangsu (one of the provinces in the YRD) were derived, (0.55, 0.75) for P_{H₂O₂}/P_{HNO₃}, (0.81, 1.35) for the surface ratio of HCHO/NO₂, (0.38, 0.60) for HCHO/NO_y, and (8.2, 17.6) for NO_y, based on the relationship between the simulated indicator values and O₃ changes resulting from a 35% reduction in the VOC or NO_x emissions. The indicators along with the localized
370 thresholds were applied in other areas in the YRD, for a different simulation period, and with a combination of different locations and time to estimate the uncertainties related to the emissions and meteorology. The indicators displayed good performance in all cases, with OA values greater than 92%, while HCHO/NO_y and HCHO/NO₂ might have been susceptible to meteorological factors. However, HCHO/NO_y and HCHO/NO₂ were the most consistent with the O₃ isopleths among the four indicators and could be informative for policymakers. The P_{H₂O₂}/P_{HNO₃} ratio was less likely to attribute O₃ formation to
375 mixed sensitivity and tended to underestimate the positive sensitivity of O₃ to NO_x compared to the isopleths. In contrast, NO_y, which was not constrained by the VOC abundance, overestimated the positive response of O₃ to NO_x and underestimated the O₃-VOC sensitivity in some conditions.

Importantly, the intrinsic characteristics of the indicators as well as the methods used to obtain the thresholds affected the effectiveness of the indicators. A series of sensitivity tests were conducted to investigate the impacts with respect to the criteria
380 for the definition of VOC- or NO_x-limited grids, the amount of VOC and NO_x emission perturbations, and the method, i.e., the HDDM tool versus emission reduction, to estimate the O₃-NO_x-VOC sensitivity in the first place. The results showed that the more stringent the criteria were (i.e., with larger the O₃ sensitivity differences or lower emission reductions using a given criterion), the wider the transition intervals were. This led to more attribution to the mixed O₃ sensitivity and showed a
385 preference for concurrent control of both precursors. However, the indicator values at the VOC- and NO_x- limited grids could overlap in a large part and could not split the O₃ sensitivity when the criteria were set too low. Finally, the first-order coefficients in the HDDM alone with a specified sensitivity difference could not be used to derive thresholds of indicators in this study, while Taylor expansions with first- and second-order sensitivity coefficients could result in lower and broader threshold intervals.

390

Photochemical indicators have the advantage of identifying O₃ formation regimes promptly and are useful in policy implications. According to the case study in this work, we found that it was inappropriate to directly use the threshold of 0.35 for P_{H₂O₂}/P_{HNO₃} in the CTMs, as the value could be location-specific. More broadly, all of the indicators should be employed with specified thresholds that have been localized and thoroughly evaluated. In addition, the indicators could be different from each other. As such, it is necessary to understand the pros and cons of each indicator prior to their use.

Code and data availability

The CMAQ outputs are currently available upon request. All python codes used to create any of the figures are available upon request.

400 Author contributions

XL, MQ and JH conceived and designed the research. XL performed the simulations and analyzed the data. MQ, JH, HS and JL contributed to result discussion. XL and MQ wrote the manuscript with substantial contributions from all of the authors.

Competing interests

The authors declare that they have no conflict of interest.

405 Acknowledgments

This work was supported by the Natural Science Foundation of Jiangsu Province (BK20200815) and the National Natural Science Foundation of China (42107117, 42007187, 42021004).

410 References

- An, J., Huang, Y., Huang, C., Wang, X., Yan, R., Wang, Q., Wang, H., Jing, S. a., Zhang, Y., Liu, Y., Chen, A. J. Y., Xu, C., Qiao, L., Zhou, M., Zhu, S., Hu, Q., Lu, J., and Chen, C.: Emission inventory of air pollutants and chemical speciation for specific anthropogenic sources based on local measurements in the Yangtze River Delta region, China, *Atmos. Chem. Phys.*, 21, 2003–2025, <https://doi.org/10.5194/acp-21-2003-2021>, 2021.
- 415 Castell, N., Stein, A. F., Mantilla, E., Salvador, R., and Millán, M.: Evaluation of the use of photochemical indicators to assess ozone-NO_x-VOC sensitivity in the Southwestern Iberian Peninsula, *J. Atmos. Chem.*, 63, 73-91, <https://doi.org/10.1007/s10874-010-9158-x>, 2009.
- Chen, X., Jiang, Z., Shen, Y., Li, R., Fu, Y., Liu, J., Han, H., Liao, H., Cheng, X., and Jones, D. B.: Chinese regulations are working-why is surface ozone over industrialized areas still high? Applying lessons from northeast US air quality evolution, *Geophys. Res. Lett.*, 48, e2021GL092816, <https://doi.org/10.1029/2021GL092816>, 2021.
- 420 Cohan, D. S., Hakami, A., Hu, Y., and Russell, A. G.: Nonlinear response of ozone to emissions: Source apportionment and sensitivity analysis, *Environ. Sci. Technol.*, 39, 6739-6748, <https://doi.org/10.1021/es048664m>, 2005.
- De Marco, A., Garcia-Gomez, H., Collalti, A., Khaniabadi, Y. O., Feng, Z., Proietti, C., Sicard, P., Vitale, M., Anav, A., and Paoletti, E.: Ozone modelling and mapping for risk assessment: An overview of different approaches for human and ecosystems health, *Environ. Res.*, 211, 113048, <https://doi.org/10.1016/j.envres.2022.113048>, 2022.
- 425 Du, X., Tang, W., Cheng, M., Zhang, Z., Li, Y., Li, Y., and Meng, F.: Modeling of spatial and temporal variations of ozone-NO_x-VOC sensitivity based on photochemical indicators in China, *J. Environ. Sci.*, <https://doi.org/10.1016/j.jes.2021.12.026>, 2022.
- Duncan, B. N., Yoshida, Y., Olson, J. R., Sillman, S., Martin, R. V., Lamsal, L., Hu, Y., Pickering, K. E., Retscher, C., and Allen, D. J.: Application of OMI observations to a space-based indicator of NO_x and VOC controls on surface ozone formation, *Atmos. Environ.*, 44, 2213-2223, <https://doi.org/10.1016/j.atmosenv.2010.03.010>, 2010.
- 430 Emery, C., Liu, Z., Russell, A. G., Odman, M. T., Yarwood, G., and Kumar, N.: Recommendations on statistics and benchmarks to assess photochemical model performance, *J. Air Waste Manage.*, 67, 582-598, <https://doi.org/10.1080/10962247.2016.1265027>, 2017.
- 435 Feng, Z., Xu, Y., Kobayashi, K., Dai, L., Zhang, T., Agathokleous, E., Calatayud, V., Paoletti, E., Mukherjee, A., Agrawal, M., Park, R. J., Oak, Y. J., and Yue, X.: Ozone pollution threatens the production of major staple crops in East Asia, *Nature Food*, 3, 47-56, <https://doi.org/10.1038/s43016-021-00422-6>, 2022.
- Gao, W., Tie, X., Xu, J., Huang, R., Mao, X., Zhou, G., and Chang, L.: Long-term trend of O₃ in a mega City (Shanghai), China: Characteristics, causes, and interactions with precursors, *Sci. Total Environ.*, 603-604, 425-433, <https://doi.org/10.1016/j.scitotenv.2017.06.099>, 2017.
- 440 Gipson, G. L. and Young, J.: Process analysis, Science Algorithms of the EPA Models-3 Community Multiscale Air Quality (CMAQ) Modeling System, 1999.
- Hu, J., Chen, J., Ying, Q., and Zhang, H.: One-year simulation of ozone and particulate matter in China using WRF/CMAQ modeling system, *Atmos. Chem. Phys.*, 16, 10333-10350, <https://doi.org/10.5194/acp-16-10333-2016>, 2016.

- 445 Jiméneez, P. and Baldasano, J. M.: Ozone response to precursor controls in very complex terrains: Use of photochemical indicators to assess O₃-NO_x-VOC sensitivity in the northeastern Iberian Peninsula, *J. Geophys. Res.-Atmos.*, 109, D20, <https://doi.org/10.1029/2004JD004985>, 2004.
- Jin, X. and Holloway, T.: Spatial and temporal variability of ozone sensitivity over China observed from the Ozone Monitoring Instrument, *J. Geophys. Res.-Atmos.*, 120, 7229-7246, <https://doi.org/10.1002/2015JD023250>, 2015.
- 450 Jin, X., Fiore, A. M., Murray, L. T., Valin, L. C., Lamsal, L. N., Duncan, B., Folkert Boersma, K., De Smedt, I., Abad, G. G., and Chance, K.: Evaluating a space - based indicator of surface ozone - NO_x - VOC sensitivity over midlatitude source regions and application to decadal trends, *J. Geophys. Res.-Atmos.*, 122, 10439-10461, <https://doi.org/10.1002/2017JD026720>, 2017.
- Kwok, R. H. F., Baker, K. R., Napelenok, S. L., and Tonnesen, G. S.: Photochemical grid model implementation and application of VOC, NO_x, and O₃ source apportionment, *Geosci. Model Dev.*, 8, 99-114, <https://doi.org/10.5194/gmd-8-99-2015>, 2015.
- 455 Li, K., Jacob, D. J., Shen, L., Lu, X., De Smedt, I., and Liao, H.: Increases in surface ozone pollution in China from 2013 to 2019: anthropogenic and meteorological influences, *Atmos. Chem. Phys.*, 20, 11423-11433, <https://doi.org/10.5194/acp-20-11423-2020>, 2020.
- 460 Li, L., Hu, J., Li, J., Gong, K., Wang, X., Ying, Q., Qin, M., Liao, H., Guo, S., Hu, M., and Zhang, Y.: Modelling air quality during the EXPLORE-YRD campaign – Part II. Regional source apportionment of ozone and PM_{2.5}, *Atmos. Environ.*, 247, 118063, <https://doi.org/10.1016/j.atmosenv.2020.118063>, 2021.
- Liang, J., Jackson, B., and Kaduwela, A.: Evaluation of the ability of indicator species ratios to determine the sensitivity of ozone to reductions in emissions of volatile organic compounds and oxides of nitrogen in northern California, *Atmos. Environ.*, 40, 5156-5166, <https://doi.org/10.1016/j.atmosenv.2006.03.060>, 2006.
- 465 Liang, S., Li, X., Teng, Y., Fu, H., Chen, L., Mao, J., Zhang, H., Gao, S., Sun, Y., Ma, Z., and Azzi, M.: Estimation of health and economic benefits based on ozone exposure level with high spatial-temporal resolution by fusing satellite and station observations, *Environ. Pollut.*, 255, 113267, <https://doi.org/10.1016/j.envpol.2019.113267>, 2019.
- Liu, H., Wang, X. M., Pang, J. M., and He, K. B.: Feasibility and difficulties of China's new air quality standard compliance: PRD case of PM_{2.5} and ozone from 2010 to 2025, *Atmos. Chem. Phys.*, 13, 12013-12027, <https://doi.org/10.5194/acp-13-12013-2013>, 2013.
- 470 Liu, J., Li, X., Tan, Z., Wang, W., Yang, Y., Zhu, Y., Yang, S., Song, M., Chen, S., Wang, H., Lu, K., Zeng, L., and Zhang, Y.: Assessing the ratios of formaldehyde and glyoxal to NO₂ as Indicators of O₃-NO_x-VOC sensitivity, *Environ. Sci. Technol.*, 55, 10935-10945, <https://doi.org/10.1021/acs.est.0c07506>, 2021.
- 475 Liu, X., Zhang, Y., Xing, J., Zhang, Q., Wang, K., Streets, D. G., Jang, C., Wang, W., and Hao, J.: Understanding of regional air pollution over China using CMAQ, part II. Process analysis and sensitivity of ozone and particulate matter to precursor emissions, *Atmospheric Environment*, 44, 3719-3727, <https://doi.org/10.1016/j.atmosenv.2010.03.036>, 2010a.

- 480 Liu, X., Zhang, Y., Xing, J., Zhang, Q., Wang, K., Streets, D. G., Jang, C., Wang, W., and Hao, J.: Understanding of regional air pollution over China using CMAQ, part II. Process analysis and sensitivity of ozone and particulate matter to precursor emissions, *Atmos. Environ.*, 44, 3719-3727, <https://doi.org/10.1016/j.atmosenv.2010.03.036>, 2010b.
- Lu, C. H. and Chang, J. S.: On the indicator - based approach to assess ozone sensitivities and emissions features, *J. Geophys. Res.-Atmos.*, 103, 3453-3462, <https://doi.org/10.1029/97JD03128>, 1998.
- Lu, X., Zhang, L., Wang, X., Gao, M., Li, K., Zhang, Y., Yue, X., and Zhang, Y.: Rapid increases in warm-season surface ozone and resulting health impact in China since 2013, *Environ. Sci. Technol. Lett.*, 7, 240-247, <https://doi.org/10.1021/acs.estlett.0c00171>, 2020.
- 485 Lu, X., Hong, J., Zhang, L., Cooper, O. R., Schultz, M. G., Xu, X., Wang, T., Gao, M., Zhao, Y., and Zhang, Y.: Severe surface ozone pollution in China: A global perspective, *Environ. Sci. Technol. Lett.*, 5, 487-494, <https://doi.org/10.1021/acs.estlett.8b00366>, 2018.
- 490 Ma, M., Yao, G., Guo, J., and Bai, K.: Distinct spatiotemporal variation patterns of surface ozone in China due to diverse influential factors, *J. Environ. Manage.*, 288, 112368, <https://doi.org/10.1016/j.jenvman.2021.112368>, 2021.
- Martin, R. V., Fiore, A. M., and Van Donkelaar, A.: Space-based diagnosis of surface ozone sensitivity to anthropogenic emissions, *Geophys. Res. Lett.*, 31, <https://doi.org/10.1029/2004GL019416>, 2004.
- Murphy, J. G., Day, D. A., Cleary, P. A., Wooldridge, P. J., Millet, D. B., Goldstein, A. H., and Cohen, R. C.: The weekend effect within and downwind of Sacramento-Part I: Observations of ozone, nitrogen oxides, and VOC reactivity, *Atmos. Chem. Phys.*, 7, 5327-5339, <https://doi.org/10.5194/acp-7-5327-2007>, 2007.
- 495 Peng, Y.-P., Chen, K.-S., Wang, H.-K., Lai, C.-H., Lin, M.-H., and Lee, C.-H.: Applying model simulation and photochemical indicators to evaluate ozone sensitivity in southern Taiwan, *J. Environ. Sci.*, 23, 790-797, [https://doi.org/10.1016/s1001-0742\(10\)60479-2](https://doi.org/10.1016/s1001-0742(10)60479-2), 2011.
- 500 Qin, Y., Li, J., Gong, K., Wu, Z., Chen, M., Qin, M., Huang, L., and Hu, J.: Double high pollution events in the Yangtze River Delta from 2015 to 2019: Characteristics, trends, and meteorological situations, *Sci. Total Environ.*, 792, 148349, <https://doi.org/10.1016/j.scitotenv.2021.148349>, 2021.
- Shen, H., Sun, Z., Chen, Y., Russell, A. G., Hu, Y., Odman, M. T., Qian, Y., Archibald, A. T., and Tao, S.: Novel method for ozone isopleth construction and diagnosis for the ozone control strategy of Chinese cities, *Environ. Sci. Technol.*, 55, 15625-15636, <https://doi.org/10.1021/acs.est.1c01567>, 2021.
- 505 Sheng, L., Qin, M., Li, L., Wang, C., Gong, K., Liu, T., Li, J., and Hu, J.: Impacts of emissions along the lower Yangtze River on air quality and public health in the Yangtze River delta, China, *Atmos. Pollut. Res.*, 101420, <https://doi.org/10.1016/j.apr.2022.101420>, 2022.
- Sillman, S.: The use of NO_y, H₂O₂, and HNO₃ as indicators for ozone-NO_x-hydrocarbon sensitivity in urban locations, *J. Geophys. Res.*, 100, 14175-14188, <https://doi.org/10.1029/94JD02953>, 1995.
- 510 Sillman, S.: The relation between ozone, NO_x and hydrocarbons in urban and polluted rural environments, *Atmos. Environ.*, 33, 1821-1845, [https://doi.org/10.1016/S1352-2310\(98\)00345-8](https://doi.org/10.1016/S1352-2310(98)00345-8), 1999.

- Sillman, S.: Some theoretical results concerning O₃-NO_x-VOC chemistry and NO_x-VOC indicators, *J. Geophys. Res.*, 107, D22, <https://doi.org/10.1029/2001jd001123>, 2002.
- 515 Sillman, S., He, D., Pippin, M. R., Daum, P. H., Imre, D. G., Kleinman, L. I., Lee, J. H., and Weinstein - Lloyd, J.: Model correlations for ozone, reactive nitrogen, and peroxides for Nashville in comparison with measurements: Implications for O₃ - NO_x - hydrocarbon chemistry, *J. Geophys. Res.-Atmos.*, 103, 22629-22644, <https://doi.org/10.1029/98JD00349>, 1998.
- Skeie, R. B., Myhre, G., Hodnebrog, Ø., Cameron-Smith, P. J., Deushi, M., Hegglin, M. I., Horowitz, L. W., Kramer, R. J., Michou, M., Mills, M. J., Oliví, D. J. L., Connor, F. M. O., Paynter, D., Samset, B. H., Sellar, A., Shindell, D., Takemura, T., Tilmes, S., and Wu, T.: Historical total ozone radiative forcing derived from CMIP6 simulations, *npj Clim. Atmos. Sci.*, 3, 32, <https://doi.org/10.1038/s41612-020-00131-0>, 2020.
- 520 Sun, J., Qin, M., Xie, X., Fu, W., Qin, Y., Sheng, L., Li, L., Li, J., Sulaymon, I. D., Jiang, L., Huang, L., Yu, X., and Hu, J.: Seasonal modeling analysis of nitrate formation pathways in Yangtze River Delta region, China, *Atmos. Chem. Phys. Discuss.*, 2022, 1-37, <https://doi.org/10.5194/acp-2022-426>, 2022.
- Tan, Z., Lu, K., Jiang, M., Su, R., Dong, H., Zeng, L., Xie, S., Tan, Q., and Zhang, Y.: Exploring ozone pollution in Chengdu, southwestern China: A case study from radical chemistry to O₃-VOC-NO_x sensitivity, *Sci. Total Environ.*, 636, 775-786, <https://doi.org/10.1016/j.scitotenv.2018.04.286>, 2018.
- 525 Tang, G., Wang, Y., Li, X., Ji, D., Hsu, S., and Gao, X.: Spatial-temporal variations in surface ozone in Northern China as observed during 2009–2010 and possible implications for future air quality control strategies, *Atmos. Chem. Phys.*, 12, 2757-2776, <https://doi.org/10.5194/acp-12-2757-2012>, 2012.
- 530 Tonnesen, G. S. and Dennis, R. L.: Analysis of radical propagation efficiency to assess ozone sensitivity to hydrocarbons and NO_x: 1. Local indicators of instantaneous odd oxygen production sensitivity, *J. Geophys. Res.-Atmos.*, 105, 9213-9225, <https://doi.org/10.1029/1999JD900371>, 2000a.
- Tonnesen, G. S. and Dennis, R. L.: Analysis of radical propagation efficiency to assess ozone sensitivity to hydrocarbons and NO_x: 2. Long-lived species as indicators of ozone concentration sensitivity, *J. Geophys. Res.-Atmos.*, 105, 9227-9241, <https://doi.org/10.1029/1999JD900372>, 2000b.
- 535 Torres-Jardon, R., García-Reynoso, J. A., Jazcilevich, A., Ruiz-Suárez, L. G., and Keener, T. C.: Assessment of the ozone-nitrogen oxide-volatile organic compound sensitivity of Mexico City through an indicator-based approach: measurements and numerical simulations comparison, *J. Air Waste Manage.*, 59, 1155-1172, <https://doi.org/10.3155/1047-3289.59.10.1155>, 2009.
- Vogel, B., Riemer, N., Vogel, H., and Fiedler, F.: Findings on NO_y as an indicator for ozone sensitivity based on different numerical simulations, *J. Geophys. Res.-Atmos.*, 104, 3605-3620, <https://doi.org/10.1029/1998JD100075>, 1999.
- 540 Wang, M., Chen, W., Zhang, L., Qin, W., Zhang, Y., Zhang, X., and Xie, X.: Ozone pollution characteristics and sensitivity analysis using an observation-based model in Nanjing, Yangtze River Delta Region of China, *J. Environ. Sci.*, 93, 13-22, <https://doi.org/10.1016/j.jes.2020.02.027>, 2020a.
- 545 Wang, N., Xu, J., Pei, C., Tang, R., Zhou, D., Chen, Y., Li, M., Deng, X., Deng, T., Huang, X., and Ding, A.: Air quality during COVID-19 lockdown in the Yangtze River Delta and the Pearl River Delta: Two different responsive mechanisms to emission reductions in China, *Environ. Sci. Technol.*, 55, 5721-5730, <https://doi.org/10.1021/acs.est.0c08383>, 2021.

- Wang, P., Guo, H., Hu, J., Kota, S. H., Ying, Q., and Zhang, H.: Responses of PM_{2.5} and O₃ concentrations to changes of meteorology and emissions in China, *Sci. Total Environ.*, 662, 297-306, <https://doi.org/10.1016/j.scitotenv.2019.01.227>, 2019.
- 550 Wang, X., Zhang, Y., Hu, Y., Zhou, W., Zeng, L., Hu, M., Cohan, D. S., and Russell, A. G.: Decoupled direct sensitivity analysis of regional ozone pollution over the Pearl River Delta during the PRIDE-PRD2004 campaign, *Atmos. Environ.*, 45, 4941-4949, <https://doi.org/10.1016/j.atmosenv.2011.06.006>, 2011.
- Wang, Y., Wild, O., Chen, X., Wu, Q., Gao, M., Chen, H., Qi, Y., and Wang, Z.: Health impacts of long-term ozone exposure in China over 2013–2017, *Environ. Int.*, 144, 106030, <https://doi.org/10.1016/j.envint.2020.106030>, 2020b.
- 555 Xie, M., Zhu, K., Wang, T., Yang, H., Zhuang, B., Li, S., Li, M., Zhu, X., and Ouyang, Y.: Application of photochemical indicators to evaluate ozone nonlinear chemistry and pollution control countermeasure in China, *Atmos. Environ.*, 99, 466-473, <https://doi.org/10.1016/j.atmosenv.2014.10.013>, 2014.
- Xu, J., Huang, X., Wang, N., Li, Y., and Ding, A.: Understanding ozone pollution in the Yangtze River Delta of eastern China from the perspective of diurnal cycles, *Sci. Total Environ.*, 752, 141928, <https://doi.org/10.1016/j.scitotenv.2020.141928>, 2021.
- 560 Ye, C., Xue, C., Zhang, C., Ma, Z., Liu, P., Zhang, Y., Liu, C., Zhao, X., Zhang, W., and He, X.: Atmospheric hydrogen peroxide (H₂O₂) at the foot and summit of Mt. Tai: variations, sources and sinks, and implications for ozone formation chemistry, *J. Geophys. Res.-Atmos.*, 126, e2020JD033975, <https://doi.org/10.1029/2020JD033975>, 2021.
- 565 Ye, L., Wang, X., Fan, S., Chen, W., Chang, M., Zhou, S., Wu, Z., and Fan, Q.: Photochemical indicators of ozone sensitivity: application in the Pearl River Delta, China, *Front. Env. Sci. Eng.*, 10, 1-14, <https://doi.org/10.1007/s11783-016-0887-1>, 2016.
- Zhang, Y., Zhao, Y., Li, J., Wu, Q., Wang, H., Du, H., Yang, W., Wang, Z., and Zhu, L.: Modeling ozone source apportionment and performing sensitivity analysis in summer on the North China Plain, *Atmosphere*, 11, 992-1011, <https://doi.org/10.3390/atmos11090992>, 2020.